Oxygen permeation, mechanical and structural properties of multilayer diffusion barrier coatings on polypropylene

2010 J. Phys. D: Appl. Phys. 43 115301

(http://iopscience.iop.org/0022-3727/43/11/115301)

IOP PUBLISHING JOURNAL OF PHYSICS D: APPLIED PHYSICS

J. Phys. D: Appl. Phys. **43** (2010) 115301 (11pp) doi:10.1088/0022-3727/43/11/115301

Oxygen permeation, mechanical and structural properties of multilayer diffusion barrier coatings on polypropylene

L Körner[1], A Sonnenfeld[1], R Heuberger[2], J H Waller[3], Y Leterrier[3], J A E Månson[3] and Ph Rudolf von Rohr[1,4]

[1] Institute of Process Engineering, ETH Zurich, 8092 Zurich, Switzerland
[2] RMS Foundation, 2544 Bettlach, Switzerland
[3] Laboratoire de Technologie des Composites et Polymères (LTC), Ecole Polytechnique Fédérale de Lausanne (EPFL), 1015 Lausanne, Switzerland

E-mail: vonrohr@ipe.mavt.ethz.ch

Received 15 December 2009, in final form 3 February 2010
Published 4 March 2010
Online at stacks.iop.org/JPhysD/43/115301

Abstract
To improve temperature durability for autoclaving of SiO_x diffusion barrier coatings on polypropylene, plasma polymerized hexamethyldisiloxane (pp-HMDSO) is applied by plasma enhanced chemical vapour deposition as interlayer material and compared with results obtained with amorphous hydrogenated carbon–nitrogen (a-C : N : H) and a-Si : C : O : N : H interlayers. The influence of the O_2/HMDSO ratio on the chemical structure and related mechanical and oxygen barrier properties is investigated by fragmentation tests, dilatometry, oxygen transmission rate, internal stress and mass density measurements as well as Fourier transform infrared and x-ray photoelectron spectroscopy. Carbon-rich, polymer-like coatings with low density, low internal stress and excellent adhesive and cohesive properties are found for pp-HMDSO at the expense of barrier performance. In the SiO_x/pp-HMDSO coating a broad transition in chemical composition was observed, explaining improved mechanical properties responsible for good barrier performance after thermal cycling or autoclaving.

1. Introduction

Silicon oxide (SiO_x) coatings are extensively explored and applied as gas diffusion barrier coatings on polymers such as for instance polyethylene terephthalate (PET). Even more than PET, though, polypropylene (PP) is an interesting substrate material for the packaging industry. This is because of its inherent water vapour barrier, low density, high availability and low cost. Apart from its high oxygen permeability, one major drawback of PP as a substrate for the deposition of thin brittle oxide films is its high thermal expansion and low glass transition temperature of $20 \times 10^{-5}\,K^{-1}$ and $-18\,^{\circ}C$, respectively [1, 2]. In direct radio frequency (RF) plasma aided deposition the temperature is well above the glass temperature of PP and polymer chains are in a rubber-like state. For food or pharmaceutical packaging applications, exposure to elevated temperatures is often inevitable, e.g. during autoclaving. Here brittle SiO_x coatings tend to crack because of the thermal expansion mismatch with the consequence of a significant loss of barrier performance. For electron beam evaporated SiO_x coatings, it was observed that exposure to $60\,^{\circ}C$ is already sufficient to induce cracks and alter gas barrier performance [3]. In this regard, plasma enhanced chemical vapour deposition (PECVD) is superior to physical vapour deposition (PVD) methods due to the formation of an extended interphase with a gradient in composition between the substrate and the coating as a result of rival ablation and redeposition processes [4, 5]. Therefore, a smoother transition of material properties and good adhesion is achieved.

For further adhesion improvement and to adapt mechanical properties between the substrate and the coating,

[4] Author to whom any correspondence should be addressed.

Table 1. Deposition parameters and properties of a-C : N : H (A), a-Si : O : C : N : H (B), pp-HMDSO (C, D) and SiO_x (E–G) single layer coatings.

Layer	A	B	C	D	E	F	G
O_2/HMDSO ratio (—)	—	—	0	0	5	15	30
HMDSO flow rate (sccm)	—	2	10	2	2	2	2
N_2 flow rate (sccm)	52.5	55	—	—	—	—	—
C_2H_2 flow rate (sccm)	7.5	3	—	—	—	—	—
RF power (W)	50	75	100	100	100	100	100
Deposition rate ($nm\,min^{-1}$)	94	207	713	543	307	198	177
OTR[a] ($cm^3\,m^{-2}\,d^{-1}\,atm^{-1}$)	14	101	>2000	>2000	1142	6	5
Atomic composition	$C_{1.0} : N_{0.05}$	$Si : O_{1.0} : C_{1.5} : N_{0.2}$	$Si : O_{0.7} : C_{1.7}$	—	$Si : O_{1.6} : C_{0.4}$	$Si : O_{1.9} : C_{0.2}$	$Si : O_{1.9} : C_{0.03}$
Si 2p peak position (eV)	—	102.7	102.4	—	103.3	103.6	103.7
Si 2p fwhm (eV)	—	2.1	2.1	—	1.9	1.8	1.7
Mass density ($g\,cm^{-3}$)	—	—	1.2	1.3	1.8	2.0	2.1
Internal stress[b] (MPa)	—	—	−42	−79	−176	−271	−487
$CLTE_c$ ($10^{-6}\,K^{-1}$)	—	—	18.0	—	4.6	2.4	1.0
E_c (GPa)	—	—	4.4	—	17.4	32.8	80.0
ν_c (—)	—	—	0.30	—	0.18	0.17	0.15
Dundurs parameter α (—)	—	—	0.73	—	0.92	0.96	0.98
Normalized ERR g (—)	—	—	2.7	—	6.3	9.6	15.4
COS[c] (%)	2.7	3.8	18.4	11.4	6.2	1.2	0.9
Toughness G_c ($J\,m^{-2}$)	—	—	77	—	77	9	20
CD^c_{sat} (mm^{-1})	210	265	1334	—	406	312	242
IFSS (MPa)	—	—	162	—	65	21	28

[a] For constant deposition time of 15 × 4 s (thickness according to deposition rate).
[b] Coating thickness ≈200 nm.
[c] Coating thickness ≈120 nm.

gradient layers or multilayer approaches were proposed and investigated [6, 7]. In a multilayer approach the combination of an amorphous hydrogenated carbon–nitrogen (a-C : N : H) and an a-Si : C : O : N : H layer with a SiO_x diffusion barrier layer was shown to be capable of efficiently improving temperature durability during autoclaving [8].

In this work, a single precursor approach is followed to obtain a good compromise between temperature durability and diffusion barrier performance as an alternative to the aforementioned multilayer approach. By varying the oxygen to monomer ratio, properties of the resulting coating can be changed from polymeric to SiO_2 like [9]. Therefore, the oxygen to monomer ratio can be employed effectively to change process conditions from favourable thermo-mechanical to good diffusion barrier properties. Particularly the influence of the oxygen to monomer ratio on the barrier performance, the density, the internal stress, the cohesive and adhesive properties by means of fragmentation tests and on the chemical structure of the resulting coatings by Fourier transform infrared (FTIR) spectroscopy and x-ray photoelectron spectroscopy (XPS) is investigated.

2. Experimental

2.1. Substrate

As substrate 30 μm thick cast PP foil, provided by Profol Kunststoffe (Germany), was used. The average roughness (S_a) was determined by atomic force microscopy to <2 nm on scans of 1 × 1 μm^2. A peak fusion temperature of 160.5 °C was measured by differential scanning calorimetry. Prior to coating the circular PP samples were cleaned in an ultrasonic acetone bath.

2.2. PECVD setup

Deposition experiments were conducted in a cylindrical stainless steel PECVD apparatus which has been described in more detail in previous works [10, 11]. The PP substrate samples were placed on the powered electrode, which was capacitively coupled to a 13.56 MHz RF generator via a matching network. The powered electrode was water cooled to 25 °C, while the reactor wall, representing the grounded electrode, was heated to 50 °C. Acetylene (Pangas, 99.6%), nitrogen (Pangas, 99.999%), oxygen (Pangas, 99.999%) and hexamethyldisiloxane (HMDSO, Sigma-Aldrich, 98.5%) flow rates were controlled by MKS mass flow controllers. Oxygen, nitrogen and acetylene were introduced at the top of the reactor and HMDSO 150 mm above the substrate using annular gas distributors. Seven different single layer coatings were produced, and their process conditions and properties are summarized in table 1. For a-C : N : H (layer A) and a-Si : C : O : N : H (layer B) a mixture of C_2H_2 and N_2 and C_2H_2, N_2 and HMDSO was applied, respectively. SiO_x coatings (layers E, F and G) were deposited from O_2–HMDSO mixtures, while plasma polymerized hexamethyldisiloxane (pp-HMDSO) coatings (layers C and D) were deposited from pure HMDSO vapour. The process pressure was kept constant at 10 Pa by a butterfly valve for all coatings. In order to keep the thermal load on the PP substrate low, intervals of 4 s plasma

operation were followed by 10 s off-time. In addition, two multilayer coatings were produced, namely, SiO_x/pp-HMDSO by combining a SiO_x top layer (layer G, deposition time 15 × 4 s) with a pp-HMDSO interlayer (layer C, 3 × 4 s) and SiO_x/a-Si : C : O : N : H/a-C : N : H by combining the same SiO_x top layer with an a-Si : C : O : N : H (layer B, deposition time 3 × 4 s) and an a-C : N : H (layer A, deposition time 3 × 4 s) interlayer.

2.3. Oxygen transmission rate

The OTR was measured by a permeability tester (Ox-Tran 100, Mocon Inc.) according to DIN 53380 at 25 °C and 50% relative humidity with a measurement accuracy of approximately ±2%.

2.4. Temperature durability and autoclaving tests

To test the temperature durability, coating/PP composites were consecutively heated to 80, 100, 120 and 140 °C in a hot air oven, maintained at the corresponding temperature for 30 min, cooled down to room temperature and the OTR was determined after each step. Additionally, separate samples were tested in an autoclave (121 °C, steam, 2.1 bar) for 30 min and the OTR was measured before and after.

2.5. Dilatometry analysis

Expansion and shrinkage behaviour of uncoated PP and 180 nm thick SiO_x/PP samples of 8 × 40 mm^2, cut along and perpendicular to machine direction, was explored using a dynamic mechanical analyzer (DMA Q800, TA Instruments) in the temperature range 25–135 °C with a heating rate of 5 K min^{-1} applying a constant load of 1 mN. The change in length of the sample was measured as a function of temperature. The coefficients of linear thermal expansion (CLTE) were deduced from the initial linear part between 30 and 45 °C.

2.6. Deposition rates and mass density

Deposition rates were determined on Si wafers, which were centred on the substrate, with a variable angle spectroscopic ellipsometer (M-2000F, J A Woollam Inc.) at three angles of incidence (65°, 70° and 75°) in the range 371–995 nm. The wavelength dependence of the refractive index was approximated with a Cauchy model [10]. Reference thickness measurements were performed with a stylus profilometer (Tencor P10).

Mass densities of the coatings were calculated from the measured coating thickness and the mass was determined on 50 × 50 mm^2 glass slides.

2.7. Internal stress

The internal stress σ_i was deduced from the radius of curvature R of the substrate/coating composite applying the equation derived by Inoue and Kobatake [12] as also in [13]:

$$\sigma_i = -\frac{E_s h_s^2}{6Rh_c} \times \frac{1}{1+mn} \times \left\{1 + n(4m-1) + n^2\left[m^2(n-1) + 4m + \frac{(1-m)^2}{1+n}\right]\right\}, \quad (1)$$

where $m = E_c/E_s$ and $n = h_c/h_s$ (E_c, E_s and h_c, h_s are the coating and the substrate Young's moduli and thicknesses, respectively). E_s of the PP foil was determined by a Zwick/Roell Z005 tensile tester to 611 MPa on rectangular samples of 18 × 10 mm^2 and for E_c estimates reported in table 1 were applied. The thickness of the coatings h_c was 200 nm for all investigated compositions. R was determined from the maximum deflection d of 80 × 15 mm^2 rectangular samples placed on supports with spacing L according to $r = L^2/(8d)$. The influence of gravity on sample curvature was found to be negligible, which was checked by measuring the deflection of the same sample twice, first with coating upside and second with coating downside.

2.8. Fragmentation tests

The fragmentation test method is a reliable technique to investigate the adhesive and cohesive properties of thin, brittle coatings on polymer substrates [13]. Tests were carried out using a Rheometric Scientific Minimat tensile tester *in situ* under an optical microscope (Olympus BX 60) equipped with videoextensometry with strain accuracy better than 10^{-3}. Rectangular samples of dimensions 8 × 40 mm^2 were incrementally strained and crack patterns were analysed in terms of crack density (CD) versus true strain. The thickness of all investigated coatings was 119 ± 6 nm. The critical strain at the propagation onset of the first crack in the coating (also termed crack onset strain, COS) was derived by linear regression from the CD versus strain data at the beginning of fragmentation. The cohesive properties of the coating such as fracture toughness can be calculated from the COS and from the elastic properties of the coating. The crack density at saturation (CD_{sat}), defined as the inverse fragment length, when an increase in strain does not result in further cracks, was also determined. This value is related to the adhesive properties of the coating. Further details regarding this technique are given elsewhere [13, 14].

The toughness of the layers, G_c, was calculated assuming that it is equal to the energy release rate (ERR) at COS, G_{ss}, using the approach detailed in [15, 16]:

$$G_{ss} = \frac{\pi}{2}\bar{E}_c h_c \varepsilon^2 g(\alpha, \beta), \quad (2)$$

where

$$\bar{E}_c = E_c/(1-\nu_c^2) \quad (3)$$

is the plane strain modulus of the coating (E_c and ν_c are Young's modulus and Poisson's ratio of the coating) and $g(\alpha, \beta)$ is a function of the Dundurs parameters α and β, which describe

the elastic mismatch of the layer/substrate system. In the case of plane strain problems

$$\alpha = \frac{\bar{E}_c - \bar{E}_s}{\bar{E}_c + \bar{E}_s}, \quad (4)$$

where

$$\bar{E}_s = E_s/(1 - \nu_s^2) \quad (5)$$

is the plane strain modulus of the substrate (ν_s is Poisson's ratio of the substrate). In this work we used $\beta = \alpha/4$. E_c was estimated as a first approximation from E_{SiO_2} and $CLTE_{SiO_2}$ values for PECVD SiO_2 (80 GPa [14] and $1 \times 10^{-6}\,K^{-1}$ [17]) and the $CLTE_c$ of the coatings as follows [18]:

$$E_c = E_{SiO_2} CLTE_{SiO_2}/CLTE_c, \quad (6)$$

where $CLTE_c$ was linearly interpolated from the values for SiO_2 and pp-HMDSO ($18 \times 10^{-6}\,K^{-1}$) using the C/Si atomic ratio, derived from XPS analysis, as the variable. The same was done with Poisson's ratio, assuming that it is equal to 0.15 for SiO_2 and 0.3 for pp-HMDSO (changing these values will marginally affect the final results).

The interfacial shear strength (IFSS), which characterizes the adhesion between the inorganic coatings and the PP substrate, was derived using the perfectly plastic Kelly–Tyson model [19]:

$$IFSS = 1.337 h_c \sigma_{max} CD_{sat}, \quad (7)$$

where σ_{max} is the coating strength taken equal to $E_c \times COS$.

2.9. FTIR spectroscopy

FTIR spectroscopy was performed on Si wafers with a Perkin-Elmer Spectrum BX II FTIR system in the range 600–4000 cm^{-1} at 2 cm^{-1} resolution. For each spectrum 64 scans were collected and averaged. The coating thickness was adjusted to 1039 ± 81 nm in order to obtain a high signal-to-noise ratio.

2.10. XPS analysis

XPS was performed with a Kratos Axis Nova (Kratos Analytical, Manchester, UK). The source was monochromatic Al Kα irradiation, run at 225 W (15 kV, 15 mA). The analysed area was 700 × 300 μm^2 in general and reduced to a diameter of 110 μm for the depth profiles. The photoelectrons were detected with a hemispherical analyzer, operated in the fixed-analyzer-transmission mode with a pass energy of 40 eV for the detailed spectra and 80 eV for the survey spectra (full width at half-maximum (fwhm) for Ag $3d_{5/2}$ = 0.75 eV and 1.1 eV, respectively). The take-off angle was 90°. Charging of the samples was over-compensated with slow electrons from the neutralizer.

The sputtering was performed using argon ions accelerated with 3.8 kV. The extractor current was 100 μA. For sputter cleaning of the reference samples, an area of 3 × 3 mm^2 was sputtered for 30 s. For sputter depth profiling, the sputtered area was 2.5 × 2.5 mm^2, resulting in a sputter rate of 15 nm min^{-1} for a Ta_2O_5 reference sample.

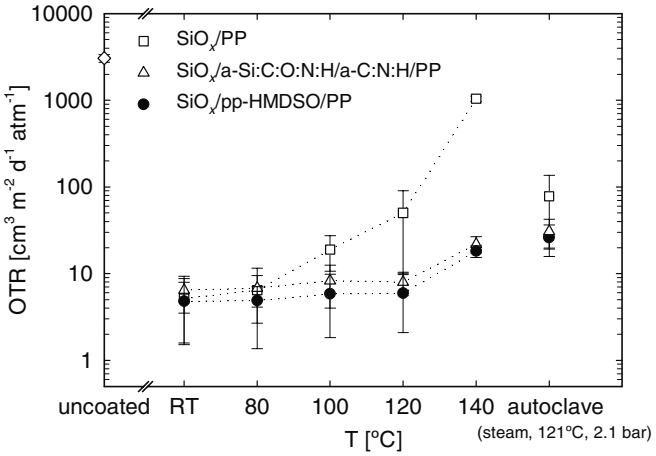

Figure 1. OTR of single and multilayered coatings on PP after deposition, after 30 min at 80, 100, 120, 140 °C and after 30 min autoclaving at 121 °C and 2.1 bar of steam. Deposition conditions of SiO_x/pp-HMDSO (layer G/C) and of SiO_x/a-Si : C : O : N : H/a-C : N : H (layer G/B/A) are summarized in table 1.

The residual pressure in the spectrometer was below 1×10^{-6} Pa for the reference samples and below 5×10^{-6} Pa during the sputter depth profiling. The system was calibrated according to ISO 15472 : 2001 and the accuracy was better than ±0.05 eV.

The spectra were analysed using the CasaXPS software (V2.3.14, Casa Software Ltd, UK). Peak shifting was corrected by referencing aliphatic carbon to 285.0 eV [20]. The peak fitting was performed after subtraction of an iterated Shirley background [21]. The quantitative composition was calculated by correcting the peak areas by the transmission function and the sensitivity factors given by Kratos assuming a homogeneous compound.

A SiO_2 reference sample was prepared by wet thermal oxidation of a Si wafer at 1000 °C for 420 min in water vapour and oxygen.

3. Results and discussion

3.1. Dry heat and autoclaving tests

In figure 1 OTR results of the dry heat and autoclaving tests of the SiO_x/pp-HMDSO/PP multilayer coating are shown and compared with results of a SiO_x/PP single layer coating and an SiO_x/a-Si : O : C : N : H/a-C : N : H/PP multilayer coating. With respect to the high OTR of the PP substrate of approximately 3100 $cm^3\,m^{-2}\,d^{-1}\,atm^{-1}$, an excellent barrier performance was obtained with all tested single and multilayer coatings with barrier improvement factors (BIF = $OTR_{uncoated}/OTR$) exceeding 500. Up to 100 °C all coatings retained their good barrier performance. After 30 min of exposure to 120 °C, the SiO_x coating without interlayer showed initial deterioration of barrier properties. Exposure to 140 °C resulted in severe loss of the barrier performance of the single SiO_x coating and the formation of cracks in the coating, perpendicular to the machine direction of the polymer, could be evidenced by optical microscopy [8, 22].

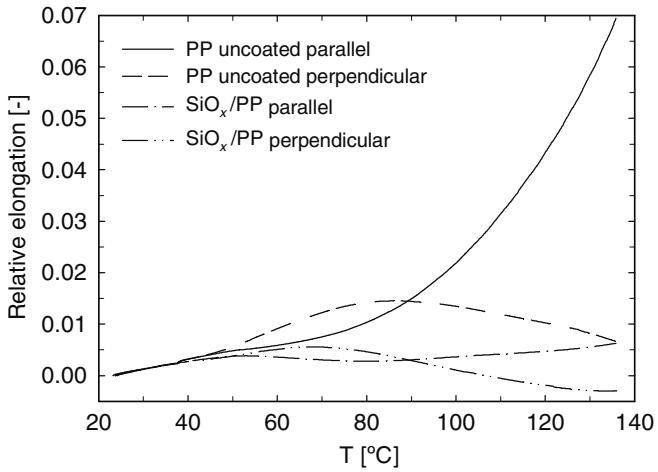

Figure 2. Dilatometry analysis of uncoated and SiO_x coated 30 μm PP foil parallel and perpendicular to the machine direction.

Exposure of the SiO_x/pp-HMDSO/PP coating to 140 °C leads only to a minor increase in the OTR to 18 $cm^3\,m^{-2}\,d^{-1}\,atm^{-1}$ as the pp-HMDSO interlayer prevents the SiO_x coating from cracking. Alternatively, a-C : N : H and a-Si : C : O : N : H can be applied as interlayer materials as shown previously. A comparison of the results shows very similar behaviour for the two multilayer coatings with only slightly superior barrier performances of the SiO_x/pp-HMDSO/PP coating. Autoclaving at 121 °C in 2.1 bar of steam for 30 min affected the coatings less than the exposure to 140 °C in dry conditions. Therefore, the temperature and the resulting thermal expansion mismatch seems to be the crucial reason for barrier performance deterioration rather than humidity. For the investigated multilayer coatings comparable low OTR values were obtained after autoclaving and after exposure to 140 °C.

3.2. Dilatometry analysis

The dilatation behaviour of PP and SiO_x/PP films during heating was investigated by means of DMA. The relative elongation of the films is shown in figure 2 over the temperature range 25–135 °C. The CLTE of the PP film was found to be equal to $20.0 \times 10^{-5}\,K^{-1}$ in good agreement with the literature data [1, 23], and that of SiO_x/PP was found to be $13.5 \times 10^{-5}\,K^{-1}$.

With increasing temperature, the influence of the coating on the dilation behaviour becomes more significant. The SiO_x coating prevents expansion of the PP film to a considerable extent, which is evidence for good adhesion and cohesion of the coating. A similar deviation is also observed for PET and SiO_x/PET films above the glass transition temperature of PET, where the shrinkage is reduced by the coating [13]. Comparing the elongation for the different orientations of the PP substrate with respect to its machine direction shows remarkable anisotropic behaviour. In the machine direction a high elongation of several per cent is observed, while at high temperatures a slight shrinkage is noticed perpendicular to the machine direction. Therefore, a high thermal tensile stress is induced in the machine direction. This is the reason for the observed cracks, formed in the brittle SiO_x coating perpendicular to the machine direction after extended exposure to 140 °C, compromising barrier performance as shown in figure 1.

Polymeric interlayers may act as buffer layers for the thermal expansion and, therefore, prevent the SiO_x diffusion barrier layer from cracking. For pp-HMDSO a CLTE of $18 \times 10^{-6}\,K^{-1}$ is reported [24]. This value is between the CLTE of the PP substrate and that of SiO_2 at (0.5–1) $\times\ 10^{-6}\,K^{-1}$ [17, 25]. Applying pp-HMDSO as interlayer material between a brittle SiO_x diffusion barrier layer and the PP substrate has the advantage that only a single precursor needs to be employed. In order to change conditions for the interlayer and the barrier layer, in principle only oxygen needs to be added to the process gas mixture, while other process parameters may remain constant. Therefore, the influence of the O_2/HMDSO ratio on the mechanical and chemical properties of the resulting coatings is investigated in detail in the following.

3.3. Influence of the O_2/HMDSO ratio

In figure 3(*a*), the influence of the O_2/HMDSO ratio on the OTR and the deposition rate is shown for constant RF power, HMDSO flow rate, process pressure and deposition time of 100 W, 2 sccm, 10 Pa and 15 $\times$ 4 s, respectively. A critical O_2/HMDSO ratio, which is around 10 at these conditions, needs to be overcome in order to obtain good barrier performance. Similar trends in OTR are reported in the literature [10, 26, 27].

The deposition rate decreases strongly with increasing O_2/HMDSO ratio up to a ratio of 15. Further increase in the O_2/HMDSO results only in a minor decrease in the deposition rate. At conditions applied for the pp-HMDSO interlayer of the SiO_x/pp-HMDSO coating (10 sccm HMDSO) high deposition rates of 710 nm min^{-1} are achieved.

The dependence of the internal stress and the mass density on the O_2/HMDSO ratio is reported in figure 3(*b*). The mass density increases from 1.3 to 2.1 g cm^{-3} as the O_2/HMDSO ratio is increased from 0 to 30. Densities typically range between 1 and 2 g cm^{-3} depending on the deposition conditions [26]. The density of SiO_x obtained for O_2/HMDSO = 30 is close to that of fused silica (2.2 g cm^{-3}) and compares well with densities obtained at similar conditions [10, 28].

The internal in-plane stress is of a compressive nature in all coatings (indicated by a negative algebraic sign). Internal stresses of the same range were determined for SiO_x deposited by PVD methods on PET [13, 29]. The internal stress rises as the O_2/HMDSO ratio is increased and follows a similar trend as the mass density and the OTR. This can be ascribed to the higher fragmentation of HMDSO molecules at high O_2/HMDSO ratios due to the high abundance of atomic oxygen.

3.4. Adhesive and cohesive properties

Adhesive and cohesive properties of single layer coatings deposited with varying O_2/HMDSO ratio between 0 and 30 were determined from the measured CD with applied tensile strain (figure 4). For SiO_x coatings with best barrier properties,

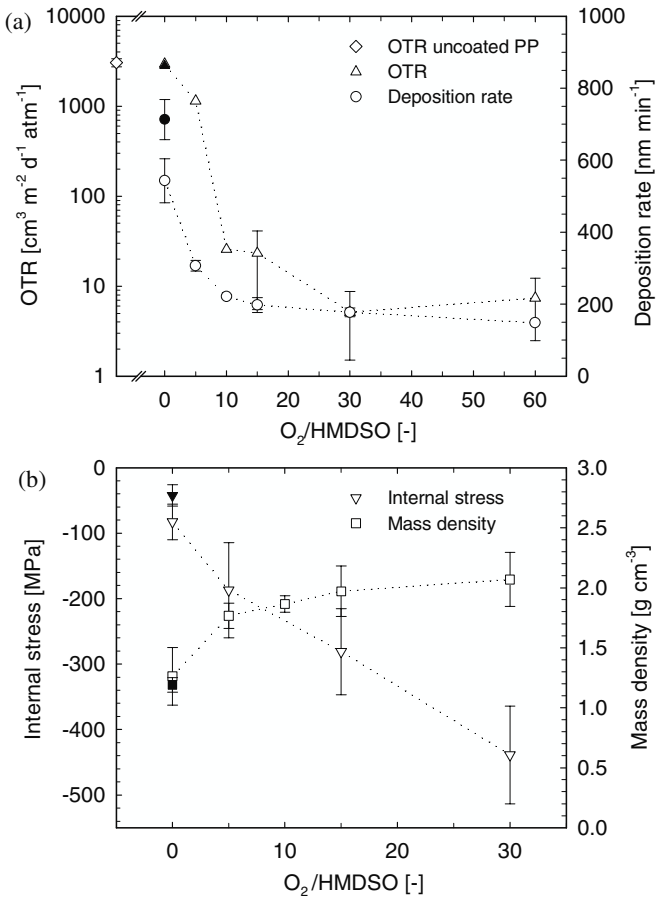

Figure 3. Influence of the O_2/HMDSO ratio on (*a*) OTR and deposition rate at constant RF power = 100 W, and deposition time = 15 × 4 s and (*b*) internal in-plane stress and mass density. HMDSO flow rate = 2 sccm (open symbols), HMDSO flow rate = 10 sccm (solid symbols).

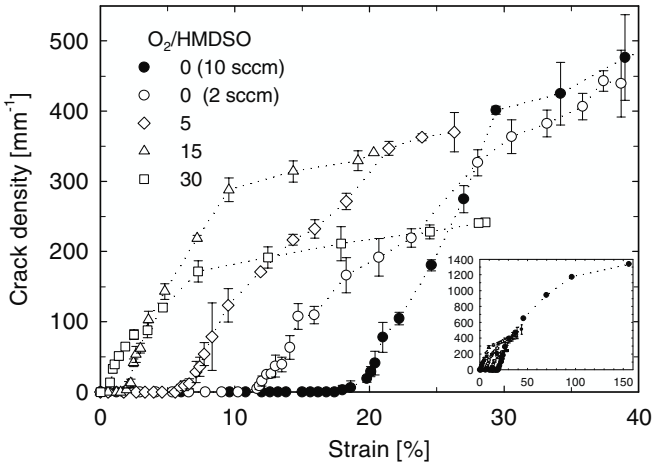

Figure 4. Crack density as a function of the applied strain of SiO_x coatings with varying O_2/HMDSO ratio between 0 and 30. RF power = 100 W, HMDSO flow rate = 2 sccm (open symbols), HMDSO flow rate = 10 sccm (solid symbols). Inset: pp-HMDSO (10 sccm HMDSO) at a highly strained position.

i.e. for O_2/HMDSO = 30, a COS of 0.9% is measured on PP, which is comparable to values reported for SiO_x on PET [13, 30, 31]. Decreasing the O_2/HMDSO ratio results in a tremendous increase in the COS up to 18% for pp-HMDSO as applied in the SiO_x/pp-HMDSO coating. The high COS shows the polymeric character of pp-HMDSO with good cohesive properties.

The E_c, ν_c and $CLTE_c$ values calculated according to equation (6) and by linear interpolation are reported in table 1. In spite of rather crude approximations, the obtained values are reasonable and would correspond to a compressive thermal stress ($E_c(CLTE_{PP} - CLTE_c)\,\Delta T$, with $\Delta T = -50$ K) of comparable magnitude to the measured values given in figure 3(*b*). Independent determination of E_c and $CLTE_c$ (using for instance indentation techniques or thermal stress analyses [32]) would clearly be useful. The Dundurs parameter α, the normalized ERR g and coating toughness G_c are also reported in table 1. The latter is in the range from 9 to 77 J m^{-2}.

Accordingly, CD_{sat} is increased with decreasing O_2/HMDSO ratio. In the inset of figure 4, the CD is shown as a function of the local strain at a highly strained position for pp-HMDSO, deposited from 10 sccm HMDSO. An extremely high CD_{sat} of 1300 mm^{-1} is observed, being evidence for excellent adhesion of pp-HMDSO to the PP substrate. Properties of the investigated coatings are summarized in table 1 and compared with the alternative interlayer materials a-C : N : H and a-Si : C : O : N : H.

The IFSS increases with increasing carbon content as reported in table 1. The IFSS of the SiO_x layer on PP is found to be equal to 28 MPa, which is almost three times higher than the shear stress at yield τ_Y of the PP substrate equal to 11 MPa. This value was derived from the measured tensile yield stress of the polymer, $\sigma_Y = 19$ MPa, using the von Mises criterion:

$$\tau_Y = \sigma_Y/\sqrt{3}. \quad (8)$$

The IFSS of the pp-HMDSO coating is as high as 162 MPa, as compared with the tensile strength of the PP substrate, close to 125 MPa. This IFSS value is likely to be overestimated, essentially due to the calculation of σ_{max} which assumes that the pp-HMDSO coating is fully elastic up to strains as high as its COS equal to 18%. A very high IFSS implies that the pp-HMDSO/PP interface is capable of strain hardening, and this is in fact visible in figure 4, where tensile failure of the pp-HMDSO coating still operates at strain levels beyond 150%.

3.5. FTIR spectroscopy

FTIR spectra of coatings deposited from O_2–HMDSO mixtures with varying O_2/HMDSO ratio between 0 and 60 are depicted in figure 5(*a*). With increasing O_2/HMDSO ratio vibrations of carbon containing groups, such as C–H in CH_2 and CH_3 at 2880, 2900 and 2960 cm^{-1} or in $Si(CH_3)_x$ at 810, 840, 880 and 1270 cm^{-1}, are reduced and disappear for O_2/HMDSO $\geqslant$30. Similar behaviour is observed for the absorption at around 2250 cm^{-1}, which is characteristic for the Si–H stretching vibration. The position of the absorption maximum is shifted towards higher wavenumbers from 2145 to 2241, 2258 and 2274 cm^{-1} as the O_2/HMDSO ratio is increased from 0 to 5, 15 and 30. It is known that the Si–H stretching frequency shifts towards higher frequencies with

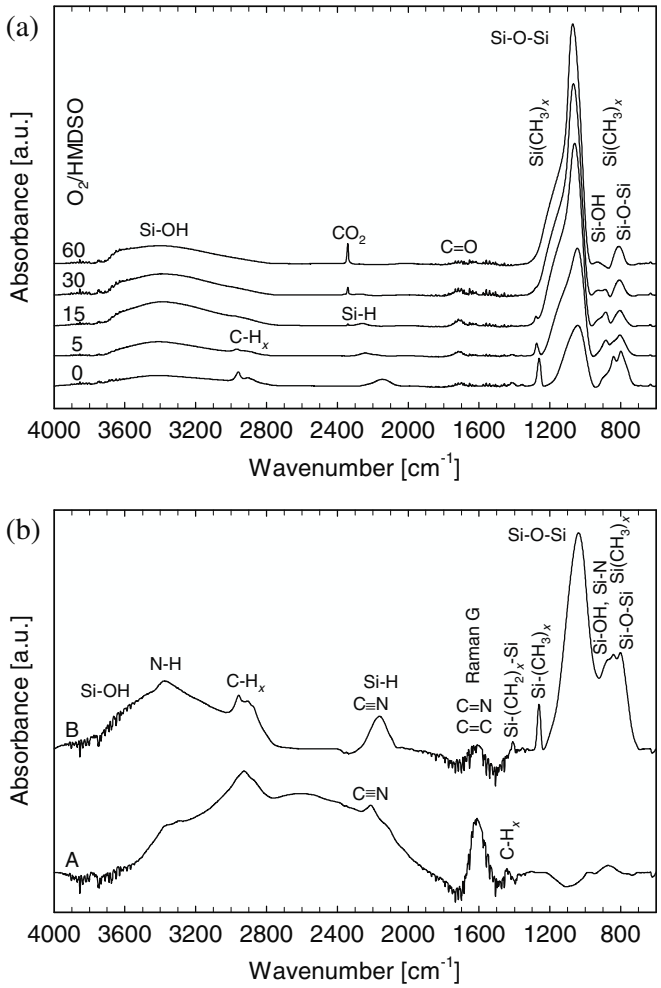

Figure 5. FTIR spectra of (*a*) SiO_x coatings with varying O_2/HMDSO ratio from 0 to 60 at constant RF power = 100 W and HMDSO flow rate = 2 sccm and (*b*) (A) a-C : N : H, (B) a-Si : C : O : N : H.

increasing sum of electronegativity of the atoms or groups bonded to the silicon [33, 34]. The stretching frequencies of the silicon monohydrates H–SiC_3, H–$SiOC_2$, H–SiO_2C and H–SiO_3 were calculated to 2135 cm^{-1}, 2185 cm^{-1}, 2234 cm^{-1} and 2283 cm^{-1} with an error of $\pm$13 cm^{-1}, respectively [34]. Therefore, the observed frequency shift can be ascribed to a change in the chemical environment of the silicon in pp-HMDSO from mainly the former two monohydrates to H–SiO_3 in SiO_x with high O_2/HMDSO ratios. Absorptions around 2250 cm^{-1} were ascribed to Si–H in H–SiO_3 [35, 36] and a similar shift was observed for HMDSO derived SiO_x coatings in the literature [37]. The intensity of the Si–O–Si stretching vibration at around 1065 cm^{-1} is increased and the peak position is shifted to higher wavenumbers (from 1041 to 1068 cm^{-1}) as the O_2/HMDSO ratio is increased from 0 to 30, indicating a densification of the Si–O–Si network. Of the characteristic bands for CO_2 at 2340 and 2360 cm^{-1} only the one at the lower wavenumber is evident in the spectra with O_2/HMDSO ratios $\geqslant$15, indicating that CO_2 is incorporated during deposition and confined to small voids in the network [38]. This gives further evidence that high fragmentation of monomer molecules and complete oxidation of their methyl groups only appears for high O_2/HMDSO ratios.

In figure 5(*b*), FTIR spectra of a-C : N : H (layer A) and a-Si : C : O : N : H (layer B) are shown. Additionally to C–H_x stretching and bending vibrations at 2860, 2913, 2948 and 1440 cm^{-1}, nitrogen containing features are also observed in the spectrum of a-C : N : H (layer A). The absorption at 1600 cm^{-1} may be a convolution of C=N stretching, N–H bending and C=C stretching vibrations. At 2200 cm^{-1} a characteristic absorption for C$\equiv$N and at 3365 cm^{-1} a shoulder of the N–H stretching vibration is observed, which is superimposed by the broad CH_x stretching vibrations. As such, these two absorptions represent terminating groups, thus reducing the degree of over-constraining of the carbon network and, therefore, the internal stress in the film. A more detailed discussion of a-C(:N) : H FTIR spectra is given elsewhere [8].

The FTIR spectrum of the a-Si : C : O : N : H layer (layer B) shows, additionally to the features observed in a-C : N : H, Si containing species and resembles the spectrum of pp-HMDSO shown in figure 5(*a*). The Si–O–Si peak position is shifted down to 1030 cm^{-1} and the absorption overlaps with the absorption at 930 cm^{-1}, which can be ascribed to both the bending vibrations of Si–N and Si–OH. As well as in the spectrum of pp-HMDSO, absorptions of Si–$(CH_3)_x$ are observed at 810, 840 and 1260 cm^{-1}. A smaller absorption of C$\equiv$N at 2200 cm^{-1} is presumably superimposed by the more pronounced absorption of Si–H at 2150 cm^{-1}, which is a terminal bond as well. Therefore, a-Si : C : O : N : H shows a high carbon content, a high fraction of terminating bonds and a low degree of cross-linking with a structure similar to pp-HMDSO.

3.6. XPS analysis

Further insight into the chemical composition was gained by XPS analysis of single layer coatings and by depth profiling of the applied multilayer coatings. Figure 6 shows the detailed spectra of Si 2p, C 1s, O 1s and N 1s of the as-deposited films. Comparing spectra C–G shows a binding energy shift of the Si 2p peak from 102.4 eV for pp-HMDSO up to 103.7 eV for the SiO_x with the highest O_2/HMDSO ratio and the thermal oxide reference sample (see table 1). In the literature, the Si 2p peak of polydimethylsiloxane (PDMS) was found at 102.1 eV while in quartz it was at 103.4 eV [39]. In PDMS the silicon is bound to two carbon atoms and two oxygen atoms (SiO_2C_2 configuration), while in quartz silicon is bound to four oxygen atoms (SiO_4 configuration). A comparison of the Si 2p peak positions with these values suggests that in pp-HMDSO the PDMS-like SiO_2C_2 and the SiO_3C configurations are prevailing, while for O_2/HMDSO ratios $\geqslant$15 almost all the silicon is found in the highly oxidized SiO_4 configuration. The FWHM was 2.1 eV for the a-Si : C : O : N : H and pp-HMDSO coatings, decreased to 1.9–1.7 eV with increasing oxygen content in the process gas mixture and dropped to 1.5 eV for the oxidized silicon wafer reference sample. This supports the hypothesis that for the a-Si : C : O : N : H and pp-HMDSO coatings a mixture of Si–O and Si–C bindings is present and with increasing O_2/HMDSO ratio the amount of Si–C bindings is decreased.

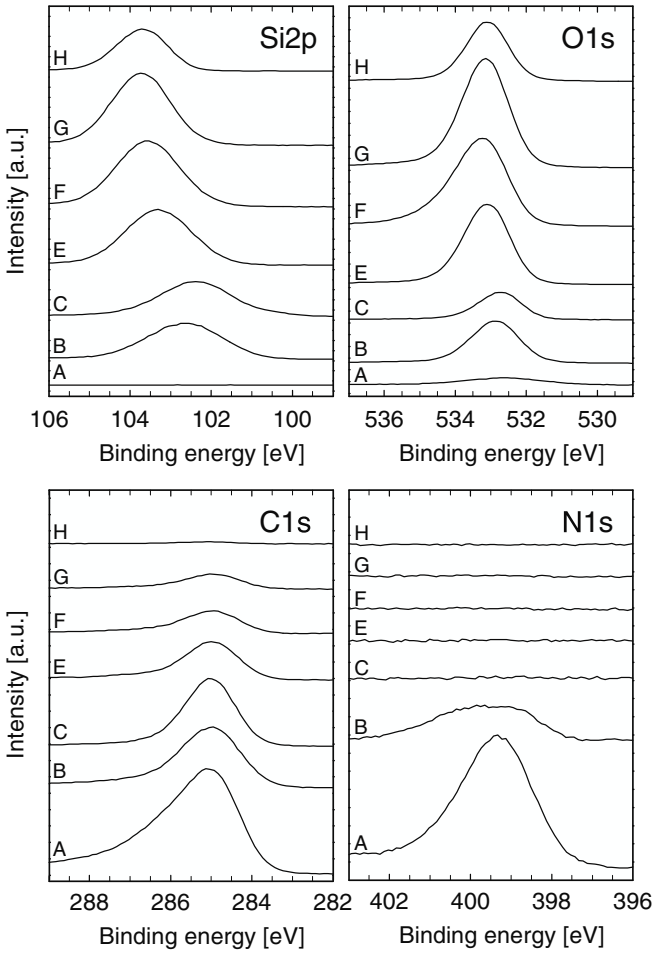

Figure 6. XPS detail spectra of Si 2p, C 1s, O 1s and N 1s of as-deposited (A) a-C : N : H, (B) a-Si : C : O : N : H, (C) pp-HMDSO (10 sccm HMDSO), (E) SiO_x (O_2/HMDSO = 5), (F) SiO_x (O_2/HMDSO = 15), (G) SiO_x (O_2/HMDSO = 30) films and (H) SiO_2 (thermal oxide).

The binding energy of oxygen was 532.8 ± 0.1 eV for the a-Si : C : O : N : H, the pp-HMDSO and the a-C : N : H coating and 533.2 ± 0.1 eV for the SiO_x coatings. These are typical values for oxygen bound to organic carbon and oxygen bound to silicon [40, 41]. The carbon signal exhibited peaks of three contributions, aliphatic carbon and carbon bound to silicon at 285.0 eV, a peak at 286.7 ± 0.2 eV due to carbon bound to oxygen or nitrogen and a peak at 288.5 ± 0.4 eV due to carbon bound to nitrogen, carbonates, esters or carboxylic groups. For the a-C : N : H and the a-Si : C : O : N : H layer, N 1s was found at 399.4 eV and at 399.7 eV, respectively, a binding energy typical for organic nitrogen [20, 42].

The Si 2p peak position of a-Si : C : O : N : H (spectrum B in figure 6) is very close to that of pp-HMDSO as shown in table 1. This supports the similarity in the chemical structure to pp-HMDSO observed by FTIR spectroscopy, but additionally carbon and nitrogen containing functionalities may be present within this material.

The influence of the O_2/HMDSO ratio on the C/Si and O/Si atomic ratios of the resulting pp-HMDSO and SiO_x films is shown in figure 7 and compared with the atomic ratios of thermal oxide grown on a Si wafer. The as-deposited samples

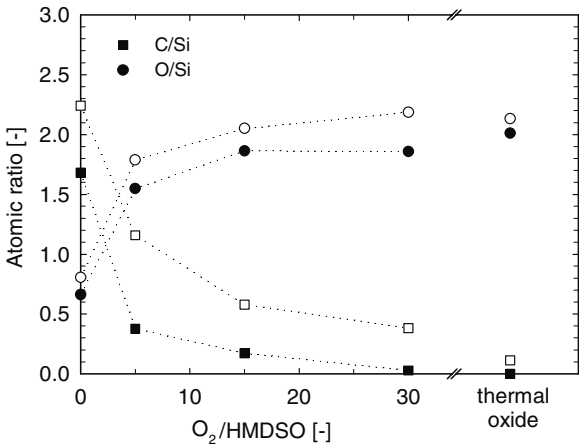

Figure 7. C/Si and O/Si atomic ratios from XPS analysis of as-deposited (open symbols) and sputter-cleaned samples (solid symbols).

showed higher C/Si and O/Si ratios than the sputter-cleaned films. The O/Si and C/Si ratios of the thermal oxide are reduced with sputter cleaning from 2.13 and 0.11 to 2.01 and 0.00, respectively. The stoichiometric composition of SiO_2 after sputter-cleaning indicates that the sputtering procedure is adequate to remove organic surface contamination and that no selective sputtering takes place. For the PECVD deposited films the reduction in the C/Si and the O/Si atomic ratio by sputtering is more pronounced compared with the thermal oxide. This may be explained by post-deposition reactions of free radicals with hydrocarbons and residual water in the vacuum chamber of the PECVD process or the adsorption of oxygen and organic material from ambient conditions. For as-deposited pp-HMDSO a C/Si ratio of 2.2 and an O/Si ratio of 0.8 were determined. Similar ratios are reported in the literature [43]. The precursor HMDSO exhibits theoretically a C/Si ratio of 3 and an O/Si ratio of 0.5. The lower C/Si ratio compared with the monomer is related to the formation of a cross-linked hydrocarbon network by methyl group abstraction and the higher O/Si ratio to reactions of long-lived radicals in the plasma polymer with atmospheric or residual oxygen and water in the plasma chamber [43–45].

The addition of oxygen results even for a low O_2/HMDSO ratio of 5 in a significant decrease in the C/Si ratio and in an increase in the O/Si ratio. This effect is more pronounced for higher O_2/HMDSO ratios: for O_2/HMDSO = 30 films with almost no carbon and an O/Si ratio of 1.9 were obtained. The observed trend is consistent with the shift of the Si 2p peak position to higher binding energies with increasing O_2/HMDSO ratio and with results from FTIR spectroscopy, indicating an increase in the Si-O absorption in Si–O–Si at the expense of carbon containing species (C–H_x, Si$(CH_3)_x$).

XPS depth profiles of the SiO_x/pp-HMDSO/PP and the SiO_x/a-Si : C : O : N : H/a-C : N : H/PP multilayer coatings are shown in figures 8(*a*) and (*b*) and compared with a SiO_x/PP coating in figure 8(*c*). The top SiO_x layer of the SiO_x/pp-HMDSO/PP multilayer coating was found to be approximately 60 nm in thickness as determined by ellipsometry of single layer films applying the same deposition parameters on Si wafers. In the bulk of the SiO_x top layer,

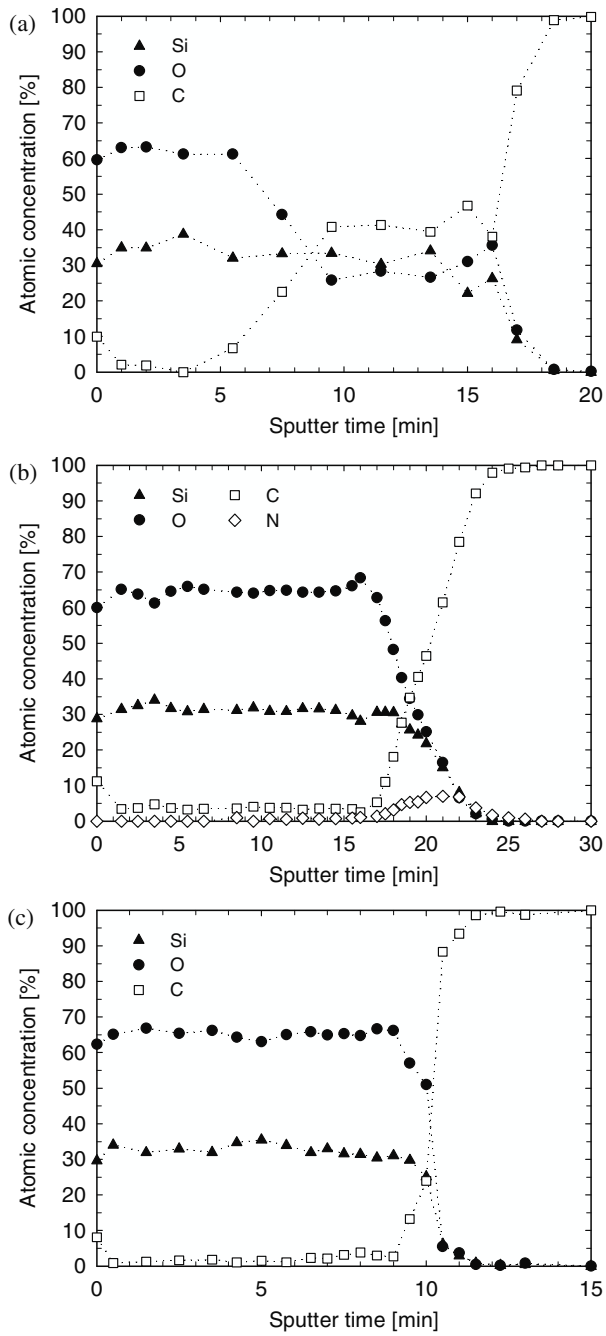

Figure 8. XPS depth profiles of (*a*) SiO_x/pp-HMDSO (layer G/C), (*b*) SiO_x/a-Si : C : O : N : H/a-C : N : H (layer G/B/A) multilayer coatings and (*c*) a SiO_x (layer G) coating on PP.

constant atomic concentrations close to those of the sputter-cleaned SiO_x reference sample with O_2/HMDSO = 30 were obtained. Between the SiO_x and the pp-HMDSO layer a broad gradual transition in chemical composition was observed. The formation of a similar interphase for SiO_x deposited on a carbon-rich layer is reported in the literature and ascribed to rival etching/redeposition processes [5]. This gradual interphase provides a smooth transition of material properties from the organic pp-HMDSO layer to the inorganic SiO_x layer. The pp-HMDSO layer shows a high constant carbon content of approximately 40% resulting in a slightly lower C/Si ratio and a higher O/Si ratio compared with the sputter-cleaned pp-HMDSO reference sample. Higher sputter rates by a factor of 1.5 are reported for pp-HMDSO compared with SiO_x in the literature [5]. This agrees well with the respective sputter times of the SiO_x and the pp-HMDSO layer and the measured thickness of approximately 130 nm of the pp-HMDSO layer by means of ellipsometry and profilometry on a reference sample produced under the same conditions. At the pp-HMDSO/PP substrate transition a gradual change in composition is observed as well. The thickness of this interphase is related to the substrate roughness [28]. In this case the interphase is rather thin affirming that the surface of the PP foil is smooth ($S_a < 2$ nm). In figure 8(*c*) the XPS depth profile of SiO_x/PP (layer G) deposited applying the same deposition time as in the SiO_x/pp-HMDSO/PP coating is shown. Similar atomic concentrations are obtained as in the top layers of the multilayer coatings. Between the SiO_x coating and the PP substrate a sharp transition in atomic composition is observed with a thin interphase comparable to the pp-HMDSO/PP substrate transition in SiO_x/pp-HMDSO/PP.

For the depth profile of the SiO_x/a-Si : C : O : N : H/a-C : N : H/PP multilayer coating, the original thickness of the SiO_x barrier layer (layer G) of approximately 180 nm was applied. The a-C : N : H was kept as thin as possible due to the low deposition rate of a-C : N : H and its brownish appearance, which becomes noticeable for thick layers. As a consequence of the rival etching/redeposition processes, it is impossible to distinguish the thin a-C : N : H and a-Si : C : O : N : H layers of approximately 19 and 45 nm as would be expected for the applied deposition time of 3 × 4 s, respectively. Moreover, a gradual transition with steadily decreasing silicon, increasing carbon content and a maximum in nitrogen content of 7% is observed.

4. Conclusions

To improve temperature durability during autoclaving, a pp-HMDSO interlayer proved to be efficient in preventing the SiO_x diffusion barrier layer from cracking as alternative to other interlayer materials. After exposure to 140 °C only a minor loss of barrier performance from 5 to 18 $cm^3\,m^{-2}\,d^{-1}\,atm^{-1}$ is observed, while for the corresponding SiO_x coating without interlayer this results in almost complete loss of barrier performance to 1040 $cm^3\,m^{-2}\,d^{-1}\,atm^{-1}$ due to the formation of cracks. These cracks are formed perpendicular to the machine direction of the PP substrate, for which the highest relative elongation of up to 7% at 130 °C is observed by means of dilatometry analysis. The thermal expansion is significantly reduced by deposition of a SiO_x coating, which is evidence for good adhesive and cohesive properties of the coating.

Plasma polymerized HMDSO is advantageous as interlayer over a-C : N : H and a-Si : C : O : N : H due to its much higher deposition rate of 710 nm min^{-1}. Furthermore, the SiO_x/pp-HMDSO coating can be deposited with HMDSO as the only precursor at constant RF power by simply adding oxygen in a one-stage process. Reducing the O_2/HMDSO ratio changes the coating properties significantly.

At high oxygen dilution, brittle, SiO_2-like coatings with high mass and network density, high compressive stress and good barrier performance are obtained. For O_2/HMDSO = 30 an increase in the O_2/HMDSO ratio does not succeed in providing further improvement of barrier performance. Under these conditions the coating is virtually carbon free with an atomic composition of $SiO_{1.9}$. A high density of 2.1 g cm^{-3} and a high compressive stress of −487 MPa is determined under these conditions accompanying a low COS of only 0.9%.

Pure HMDSO feed to the discharge results in polymer-like coatings with a high carbon content showing an atomic composition of $SiO_{0.7}C_{1.7}$. FTIR spectra revealed pronounced absorptions of CH_x, $Si(CH_3)_x$ and Si–H species, while the Si–O–Si peak intensity is drastically reduced and the peak position shifted towards lower wavenumbers, indicating low Si–O network density as a result of low monomer fragmentation. In pp-HMDSO a low internal stress is measured, accompanied by a low mass density of 1.2 g cm^{-1}. Fragmentation tests on pp-HMDSO coatings indicated a high COS of 18% and a high CD_{sat} of 1300 mm^{-1}. Estimates of the fracture toughness and IFSS are found to be close to 80 J m^{-2} and 160 MPa, i.e. four and six times higher than the respective values for the SiO_x coating. Therefore, the obtained pp-HMDSO coatings show excellent cohesive and adhesive properties. Unfortunately, these properties of pp-HMDSO are achieved at the expense of barrier performance. The XPS depth profile of the SiO_x/pp-HMDSO coating shows a broad gradual transition in chemical composition between pp-HMDSO and SiO_x because of rival etching/redeposition processes and a not so broad transition between the PP substrate and pp-HMDSO due to the smooth substrate surface. This provides a gradual transition of material properties and good adhesion.

Therefore, pp-HMDSO and SiO_x in a multilayer coating combine advantageous properties of both materials and present a promising approach for packaging applications, where coatings are subjected to thermal cycling.

Acknowledgments

The authors are indebted to B Malisova and Professor M Textor from the Laboratory for Surface Science and Technology (LSST, ETH Zurich) for providing access to the ellipsometer and the Center of Mechanics at the Institute of Mechanical Systems (IMES, ETH Zurich) for the access to the surface profiler. Furthermore, funding by the Commission for Technology and Innovation (CTI), Bern, Switzerland, is gratefully acknowledged.

References

[1] Crespi G and Luciani L 1981 *Kirk-Othmer Encyclopedia of Chemical Technology* 3rd edn vol 16 ed H F Mark *et al* (New York: Wiley) pp 453–69
[2] Reding F P 1956 *J. Polym. Sci.* **21** 547–9
[3] Henry B M, Norenberg H, Dinelli F, Grovenor C R M, Briggs G A D, Tsukahara Y and Miyamoto T 1999 *Chem. Eng. Technol.* **22** 1010–1
[4] Dennler G, Houdayer A, Raynaud P, Séguy I, Ségui Y and Wertheimer M R 2003 *Plasma Polym.* **8** 43–59
[5] Hegemann D, Schütz U and Oehr Ch 2005 *Plasma Processes and Polymers* ed R d'Agostino *et al* (Weinheim: Wiley–VCH) pp 23–37
[6] Hegemann D, Brunner H and Oehr Ch 2002 *Proc. 45th SVC Ann. Technical Conf. (Lake Buena Vista, FL)* pp 174–8
[7] Schwarzer N 2000 *Surf. Coat. Technol.* **133-134** 397–402
[8] Körner L, Sonnenfeld A and Rudolf von Rohr Ph 2009 *Plasma Process. Polym.* **6** S660–S4
[9] Lamendola R, d'Agostino R and Fracassi F 1997 *Plasma Polym.* **2** 147–64
[10] Grüniger A, Bieder A, Sonnenfeld A, Rudolf von Rohr Ph, Müller U and Hauert R 2006 *Surf. Coat. Technol.* **200** 4564–71
[11] Sonnenfeld A, Bieder A and Rudolf von Rohr Ph 2006 *Plasma Process. Polym.* **3** 606–17
[12] Inoue Y and Kobatake Y 1958 *Appl. Sci. Res.* A **7** 314
[13] Leterrier Y, Wyser Y and Månson J A E 2001 *J. Adhes. Sci. Technol.* **15** 841–65
[14] Leterrier Y, Wyser Y, Månson J A E and Hilborn J 1994 *J. Adhes.* **44** 213–27
[15] Andersons J, Modniks J, Leterrier Y, Tornare G, Dumont P and Månson J A E 2008 *Theor. Appl. Fract. Mech.* **49** 151–7
[16] Beuth J L 1992 *Int. J. Solids Struct.* **29** 1657–75
[17] Zhao J-H, Ryan T, Ho P S, McKerrow A J and Shih W-Y 1999 *J. Appl. Phys.* **85** 6421–4
[18] Ashby M F 1989 *Acta Metall.* **37** 1273–93
[19] Kelly A and Tyson W R 1965 *J. Mech. Phys. Solids* **13** 329–50
[20] Beamson G and Briggs D 1992 *High Resolution XPS of Organic Polymers* (Chichester, UK: Wiley)
[21] Shirley D A 1972 *Phys. Rev.* B **5** 4709
[22] Inagaki N and S. T 2000 *J. Appl. Polym. Sci.* **78** 2389–97
[23] Degamber B, Winter D, Tetlow J, Teagle M and Fernando G F 2004 *Meas. Sci. Technol.* **15** L5–L10
[24] Akira M and Yoshihiro A 1982 *J. Appl. Polym. Sci.* **27** 2139–50
[25] Sunami H, Itoh Y and Sato K 1970 *J. Appl. Phys.* **41** 5115–17
[26] Agres L, Ségui Y, Delsol R and Raynaud P 1996 *J. Appl. Polym. Sci.* **61** 2015–22
[27] Lamendola R and d'Agostino R 1998 *Pure Appl. Chem.* **70** 1203–8
[28] Hegemann D, Vohrer U, Oehr Ch and Riedel R 1999 *Surf. Coat. Technol.* **116–119** 1033–6
[29] Robic J Y, Leplan H, Pauleau Y and Rafin B 1996 *Thin Solid Films* **290–291** 34–9
[30] Bieder A, Gondoin V, Leterrier Y, Tornare G, Rudolf von Rohr Ph and Månson J A E 2007 *Thin Solid Films* **515** 5430–8
[31] Yanaka M, Kato Y, Tsukahara Y and Takeda N 1999 *Mater. Res. Soc. Symp. Proc.* **555** 33–8
[32] Chiang M Y M, Chiang C K and Wu W L 2002 *J. Eng. Mater. Technol.* **124** 274–7
[33] Lucovsky G 1979 *Solid State Commun.* **29** 571–6
[34] Tsuchida H, Kamata I and Izumi K 1997 *Japan. J. Appl. Phys.* **36** L699
[35] Han S M and Aydil E S 1996 *J. Vac. Sci. Technol.* A **14** 2062–70
[36] Ogata Y, Niki H, Sakka T and Iwasaki M 1995 *J. Electrochem. Soc.* **142** 195–201
[37] Aumaille K, Vallée C, Granier A, Goullet A, Gaboriau F and Turban G 2000 *Thin Solid Films* **359** 188–96
[38] Theil J A, Brace J G and Knoll R W 1994 *J. Vac. Sci. Technol.* A **12** 1365–70
[39] Alexander M R, Short R D, Jones F R, Michaeli W and Blomfield C J 1999 *Appl. Surf. Sci.* **137** 179–83
[40] Görlich E, Haber J, Stoch A and Stoch J 1980 *J. Solid State Chem.* **33** 121–4

[41] Gardner S D, Singamsetty C S K, Booth G L, He G-R and Pittman C U 1995 *Carbon* **33** 587–95
[42] Moulder J F, Stickle W F, Sobol P E and Bomben K D 1995 *Handbook of X-Ray Photoelectron Spectroscopy* (Eden Prairie, MN, USA: Perkin-Elmer, Physical Electronics Division)
[43] Balkova R, Zemek J, Cech V, Vanek J and Prikryl R 2003 *Surf. Coat. Technol.* **174–175** 1159–63
[44] Yasuda H, Bumgarner M O, Marsh H C and Morosoff N 1976 *J. Polym. Sci. Polym. Chem. Edn* **14** 195–224
[45] Zuri L, Silverstein M S and Narkis M 1996 *J. Appl. Polym. Sci.* **62** 2147–54